

Published in final edited form as:

*Oncogene*. 2015 September 3; 34(36): 4713–4722. doi:10.1038/onc.2014.396.

## Hypoxic regulation of RIOK3 is a major mechanism for cancer cell invasion and metastasis

Dean C. Singleton<sup>1</sup>, Pegah Rouhi<sup>2</sup>, Christos E. Zois<sup>1</sup>, Syed Haider<sup>1</sup>, Ji-Liang Li<sup>1</sup>, Benedikt M. Kessler<sup>3</sup>, Yihai Cao<sup>2,4,5</sup>, and Adrian L. Harris<sup>1</sup>

<sup>1</sup>Department of Oncology, Weatherall Institute of Molecular Medicine, University of Oxford, John Radcliffe Hospital, Oxford OX3 9DS, UK

<sup>2</sup>Department of Microbiology, Tumor and Cell Biology, Karolinska Institute, 171 77 Stockholm, Sweden

<sup>3</sup>Target Discovery Institute, Nuffield Department of Medicine, University of Oxford, Roosevelt Drive, Oxford OX3 7FZ, UK

<sup>4</sup>Department of Medicine and Health Sciences, Linköping University, 581 83. Linköping, Sweden

<sup>5</sup>Department of Cardiovascular Sciences, University of Leicester and NIHR Leicester Cardiovascular Biomedical Research Unit, Glenfield Hospital, Leicester, LE3 9QP, UK

### Abstract

Hypoxia is a common feature of locally advanced breast cancers and is associated with increased metastasis and poorer survival. Stabilisation of Hypoxia-Inducible Factor-1 $\alpha$  (HIF1 $\alpha$ ) in tumours causes transcriptional changes in numerous genes that function at distinct stages of the metastatic cascade. We demonstrate that expression of RIOK3 was increased during hypoxic exposure in a HIF1 $\alpha$ -dependent manner. RIOK3 was localised to distinct cytoplasmic aggregates in normoxic cells and underwent redistribution to the leading edge of the cell in hypoxia with a corresponding change in the organisation of the actin cytoskeleton. Depletion of RIOK3 expression caused MDA-MB-231 to become elongated and this morphological change was due to a loss of protraction at the trailing edge of the cell. This phenotypic change resulted in reduced cell migration in 2D cultures and inhibition of cell invasion through 3D extracellular matrix. Proteomic analysis identified interactions of RIOK3 with actin and several actin-binding factors including tropomyosins (TPM3 and TPM4) and tropomodulin 3 (TMOD3). Depletion of RIOK3 in cells resulted in fewer and less organised actin filaments. Analysis of these filaments showed reduced association of TPM3, particularly during hypoxia, suggesting that RIOK3 regulates actin filament specialisation. RIOK3 depletion reduced the dissemination of MDA-MB-231 cells in both a zebrafish model of systemic metastasis and a mouse model of pulmonary metastasis. These findings demonstrate that RIOK3 is necessary for maintaining actin cytoskeletal organisation

Users may view, print, copy, and download text and data-mine the content in such documents, for the purposes of academic research, subject always to the full Conditions of use:[http://www.nature.com/authors/editorial\\_policies/license.html#terms](http://www.nature.com/authors/editorial_policies/license.html#terms)

*Corresponding author:* Adrian L. Harris, Department of Oncology, Weatherall Institute of Molecular Medicine, John Radcliffe Hospital, University of Oxford, Oxford, OX3 9DS, United Kingdom. Phone: 44-1865-222457; Fax: 44-1865-222431; [aharris.lab@imm.ox.ac.uk](mailto:aharris.lab@imm.ox.ac.uk).

The authors declare no conflict of interest.

required for migration and invasion, biological processes that are necessary for hypoxia-driven metastasis.

## Keywords

---

## Introduction

Basal-like breast cancers are characterised by higher rates of relapse and distant metastasis than other breast cancer subtypes.<sup>1</sup> Hypoxic regions ( $pO_2 < 2.5$  mmHg; equivalent to  $\sim 0.3\%$   $O_2$ ) are a common feature of locally advanced breast tumours but are not detected in normal breast tissue.<sup>2</sup> Numerous studies have shown that the existence of intratumoural hypoxia is associated with poor prognosis (reviewed by Rundqvist and Johnson).<sup>3</sup> In particular, hypoxia is correlated with an increased occurrence of metastasis of breast cancers.<sup>4, 5</sup> Stabilisation of hypoxia-inducible transcription factors (HIF1 $\alpha$  and HIF2 $\alpha$ ) occurs in hypoxic cells of tumours. Transcription of HIF target genes promote diverse steps of the metastatic cascade including extracellular matrix remodelling (MMP, LOX and P4HA family members<sup>6-8</sup>), vascular intra- and extravasation (L1CAM and ANGPTL4<sup>9</sup>), epithelial-mesenchymal transition (E-cadherin and SNAIL<sup>10</sup>) and cell invasiveness (HGF/MET<sup>11</sup>).

Cell migration depends on dynamic and co-ordinated organisation of the actin cytoskeleton. Growing evidence suggests that protrusions at the leading edge and generation of actomyosin contraction forces in the cell are achieved by distinct specialised subsets of actin filaments (F-actin).<sup>12, 13</sup> A number of actin filament modifying proteins are involved, carrying out specialised processes including nucleation, branching and severing. The association of tropomyosins with F-actin increases filament stability and coordinates access of other actin-interacting factors.<sup>14, 15</sup> Tropomyosins are particularly important in promoting sustained migration of cells by increasing recruitment of myosin II to F-actin resulting in production of strong actomyosin-mediated contractile force.<sup>16</sup>

*Right Open reading frame (RIO) kinases are a conserved family of atypical serine/threonine protein kinases. The RIO kinase family consists of three members (RIOK1-3). Each member has been implicated in processing of the pre-40S ribosomal subunit.<sup>17-19</sup> In addition, RIOK3 has been implicated in cell invasion, although the mechanism has not been well defined.<sup>20</sup> We observed increased RIOK3 expression in a gene expression analysis of MCF7 cells exposed to severe hypoxia ( $< 0.01\%$   $O_2$ ) for 24 h.<sup>21</sup> These observations led us to hypothesise that RIOK3 may be involved in hypoxic invasion and metastasis. In this report we demonstrate that RIOK3 expression is increased in hypoxia in a HIF1 $\alpha$ -dependent manner. RIOK3 promotes reorganisation of the actin cytoskeleton increasing both cell migration and invasion and depletion of RIOK3 strongly reduces the metastatic potential of cells *in vivo*.*

## Results

### RIOK3 expression is increased during hypoxic exposure

Analysis of RIOK3 expression using the Metabric cohort showed that basal-like breast cancers have increased expression of RIOK3 compared with luminal A, luminal B, Her2 positive and normal-like breast cancer subtypes and normal breast tissue (Fig S1A-B).<sup>22</sup> The basal-like subset of breast cancers has been reported to possess high activity of the HIF1 $\alpha$ /ARNT pathway.<sup>23</sup> Additional analysis of the basal-like subset (n = 331) demonstrated that RIOK3 expression was correlated with a validated 51-gene hypoxia signature, suggesting that RIOK3 expression in these breast cancers may be regulated by hypoxia ( $\rho = 0.42$ ; Fig S1C).<sup>24</sup> In the Metabric cohort high expression of RIOK3 was associated with poorer overall survival prognosis (Fig S1D).

To understand the influence of hypoxia on RIOK3 expression MDA-MB-231 cells were exposed to 0.1% O<sub>2</sub> for 0-72 h (Fig 1A). A time dependent increase in RIOK3 mRNA was observed following hypoxic exposure, with levels increasing  $2.9 \pm 0.62$ -fold after 72 h exposure (mean  $\pm$  SEM, n = 3). The magnitude of RIOK3 hypoxic up-regulation was lower than that observed for characterised HIF target genes CA9 and ADM but similar to the fold change observed for SERPINE1 (Fig S2A-C). RIOK3 protein levels were also modestly increased in hypoxia peaking at 24 h before falling back to basal levels by 72 h (Fig 1B). This hypoxic increase in RIOK3 expression was also observed in MCF7, HCT 116 and U-87 MG cells, although the kinetics and amplitude of induction were variable between cell lines (Fig S3A-C).

To investigate the role of HIF in this hypoxic induction, knockdown of either HIF1 $\alpha$ , HIF2 $\alpha$  or HIF1 $\alpha$  and HIF2 $\alpha$  were undertaken using siRNA (Fig 1C-D). Knockdown of HIF1 $\alpha$ , but not HIF2 $\alpha$ , suppressed the hypoxic up-regulation of RIOK3 at both mRNA and protein level. Minimal additional effect was observed when both HIF1 $\alpha$  and HIF2 $\alpha$  were co-depleted suggesting that HIF1 $\alpha$  is predominantly responsible for the hypoxic induction of RIOK3. Control hypoxic genes responded as reported with CA9 displaying exclusive HIF1 $\alpha$  regulation whereas ADM and SERPINE1 demonstrated greater dependence on HIF2 $\alpha$  (Fig S2D-F).<sup>25-27</sup> In addition, pharmacological stabilisation of HIF using a prolyl hydroxylase inhibitor, dimethyloxalylglycine (DMOG), increased expression of RIOK3, further supporting the hypothesis that RIOK3 is a HIF1 $\alpha$  target gene (Fig S3D).

### RIOK3 undergoes relocalisation in hypoxic cells

We hypothesized that the minor up-regulation that occurs in hypoxia is unlikely to result in increased overall activity but rather suggests a necessary function for RIOK3 during hypoxic conditions. To test this hypothesis, confocal microscopy of RIOK3 stained cells was performed (Fig 2A). Immunofluorescent staining of RIOK3 in cells demonstrated cytoplasmic localisation, consistent with published observations.<sup>17</sup> Cells in normoxic culture displayed prominent spherical RIOK3 stained aggregates at the cell periphery (arrowheads) with less intense, grainy staining in the remaining cytoplasm. When exposed to hypoxia for 24 h these aggregates disappeared and the RIOK3 stain became more diffuse throughout the

cytoplasm with some cells displaying a band of intense staining adjacent to the leading edge (arrowheads).

### **RIOK3 expression is required for cell migration and invasion**

To understand the function of RIOK3, MDA-MB-231 cells were transduced with lentivirus expressing shRNA to RIOK3 (shRIOK3). This resulted in approximately 65% knockdown of RIOK3 protein expression (Fig 2B). Dishes seeded with a low density of shCon-expressing cells formed a scattered homogeneous pattern of growth after 1 week in culture consistent with the migratory nature of these cells (Fig 2C). In contrast, most shRIOK3 cells formed tight colonies (arrowheads), suggesting a defect in cell migration. When observed at higher magnification cells expressing shCon were smaller and rounder compared to the elongated phenotype observed for shRIOK3 cells (Fig S4A). To confirm these observations MDA-MB-231 cells were transfected with siRNA targeting RIOK3, resulting in approximately 90% knockdown (Fig 2D). Cells transfected with control siRNA (siCon) were small, rounded and many were observed as individual cells not in contact with others suggestive of active migration (arrowheads; Fig 2E). In contrast, cells transfected with siRIOK3 were elongated and prone to clumping with few individual cells observed away from cell clusters (arrowheads).

The modified scratch wound assay was used to determine whether the changes in cell morphology observed with knockdown of RIOK3 had an effect on cell migration (Fig 3A). Normoxic cells transfected with siCon migrated into the wound and closed  $35 \pm 2.0\%$  of the wound area at 16 h (mean  $\pm$  SEM,  $n = 4$ ). Knockdown of RIOK3 reduced normoxic cell migration resulting in  $19 \pm 5.0\%$  wound closure. Hypoxic treatment modestly stimulated cell migration producing  $42 \pm 5.9\%$  wound closure. Knockdown of RIOK3 resulted in a statistically significant reduction of hypoxic cell migration with  $17 \pm 3.0\%$  of the wound closed ( $P < 0.05$  vs. siCon normoxia and  $P < 0.01$  vs. siCon hypoxia; one-way ANOVA).

To further characterise this defect in cell migration, analysis of single cell migration was carried out in low density cell cultures (Fig 3B). Cells transfected with siCon migrated in a non-directional manner with velocity of  $0.95 \pm 0.012 \mu\text{m}/\text{min}$  (mean  $\pm$  SEM,  $n = 3$ ), in agreement with recent findings.<sup>28</sup> In contrast, migration of siRIOK3 cells was significantly slower at a rate of  $0.43 \pm 0.014 \mu\text{m}/\text{min}$  ( $P < 0.001$ ;  $t$  test). RIOK3 knockdown also reduced the maximum distance travelled from the origin from  $82 \pm 6.9 \mu\text{m}$  to  $59 \pm 4.0 \mu\text{m}$  during the 5 h observation period (Fig 3C, mean  $\pm$  SEM,  $n = 3$ ,  $P < 0.05$ ;  $t$  test).

A series of timelapse images of a single cell demonstrated the stepwise mode of cell migration utilised by these cells (Fig 3D). The siCon transfected cell formed a protrusion at the leading edge of the cell (arrowhead) and this was followed by translocation of the cell body and retraction of the trailing edge. This pattern was repeated approximately every 20-30 min producing active migration. In contrast, the siRIOK3 cell demonstrated a defect in its ability to retract the trailing edge leading to the formation of a long tail. These cells appeared to protrude a normal lamellipodium at the leading edge. Timelapse videos supported this phenotype with all siRIOK3 cells developing long projections at the trailing edge at some point during the observation period (Video S1).

The effect of RIOK3 on 3D invasion was investigated using the Boyden chamber assay (Fig 3E-F). Invasion of siRIOK3-transfected MDA-MB-231 cells through Matrigel was reduced to  $9.3 \pm 3.5\%$  of siCon invasion in normoxia (mean  $\pm$  SEM,  $n = 3$ ). Hypoxia significantly increased cell invasion by  $540 \pm 190\%$  ( $P < 0.05$ ; one way ANOVA). This effect was significantly suppressed by siRIOK3 to  $22 \pm 11\%$  of siCon normoxic invasion ( $P < 0.05$  vs. siCon hypoxia). This data both confirms the observed deficiency in 2D migration and suggests a more specific role for RIOK3 in 3D cell invasion. RIOK3 depletion had no effect on proliferation of MDA-MB-231 cells (Fig S5). Similar defects in cell migration and invasion were observed in SK-OV-3 ovarian adenocarcinoma cells following RIOK3 knockdown (Fig S6).

### **RIOK3 is required for organisation of the actin cytoskeleton**

Rio kinases from yeast and *Archaeoglobus fulgidus* are capable of serine (auto)phosphorylation *in vitro*, however, the existence/identity of substrates is currently unknown.<sup>29</sup> We utilised the analogue sensitive kinase assay to search for RIOK3 substrates.<sup>30</sup> We were unable to identify novel sites of thiophosphorylation using this method suggesting that RIOK3 is not amenable to analysis using this strategy (Fig S7). RIOK3 levels were reduced in the digitonin-permeabilised cells used in the analogue sensitive kinase assay suggesting that much of the RIOK3 has diffused out of the cell. Consistently, fluorescence recovery after photobleaching (FRAP) analysis demonstrated that GFP-RIOK3 was highly diffusible in the cytoplasm, with the exception of a few focal aggregates (Fig S8).

As an alternative approach to understand the basis of RIOK3 function in regulating cell migration, we carried out co-immunoprecipitation studies using FLAG-tagged RIOK3 coupled with tandem mass spectrometry to identify interacting species (Fig 4A). We identified a number of interacting proteins including components of the actin cytoskeleton including actins (ACTG1, ACTA2), tropomyosins (TPM3, TPM4) and tropomodulin 3 (TMOD3). Ribosomal subunits (RPS3, RPS14, RPS16, RPS18, RPS20, RPL27A, RPL30) were also identified, consistent with the reported role of RIOK3 in ribosomal biogenesis.<sup>17</sup>

To further investigate the role of RIOK3 in cytoskeletal regulation we used confocal microscopy to examine the localisation of RIOK3 and TPM3 in MDA-MB-231 cells (Fig 4B). In normoxia, TPM3 was detected in the same large cytoplasmic aggregates that contain increased levels of RIOK3 (arrowheads). During hypoxia RIOK3 redistributed away from the cell edge with a corresponding loss of visible aggregates. TPM3 followed a similar pattern of redistribution but was also observed to associate with stress fibers both through the centre of the cell (below the nucleus) and at the cell edges.

Similar studies were carried out to demonstrate the relationship between RIOK3 and F-actin (Fig 4C). In normoxia F-actin was observed as distinct perinuclear foci and as larger circular structures proximal to the cell edge with no obvious stress fibers present (arrowheads). Many of these circular associations of F-actin contained RIOK3 aggregates in the centre, suggesting an association between the two rather than direct co-localisation (Fig 4D). In hypoxia the F-actin cytoskeleton underwent reorganisation with a clear lamellipodium at the leading edge of the cell and prominent stress fibers on the flanking edges of the cell. RIOK3

aggregates dispersed, as noted earlier, and a band of more intense staining formed at the leading edge. Magnification of this region revealed a narrow approximately 1.3  $\mu\text{m}$  intense band of F-actin at the leading edge, a band of approximately 2.5  $\mu\text{m}$  that excluded F-actin behind this and then a wider 6  $\mu\text{m}$  band of F-actin further behind (Fig 4D). The two stains were mutually exclusive with the band that excludes F-actin being positive for RIOK3 and vice versa (Fig 4E). Thus the relationship observed between RIOK3 and F-actin in normoxia was also seen in hypoxia with RIOK3 positive regions mostly excluding but directly adjacent to regions of F-actin.

To understand the effect of RIOK3 on actin organisation F-actin staining was carried out in MDA-MB-231 cells transfected with siRIOK3 (Fig 5A). RIOK3 knockdown cells displayed an elongated phenotype with less F-actin staining in normoxia and even less in hypoxia, suggesting fewer actin filaments were present. Notably, both the perinuclear F-actin foci and the circular structures at the cell edge were lost following RIOK3 knockdown with an appearance of long actin filaments, possibly stress fibers. In hypoxia RIOK3 translocated away from the cell periphery and prominent stress fibers formed in these areas.

Destabilisation of the F-actin cytoskeleton in siRIOK3 cells was confirmed by analysis of globular (G) and filamentous (F) actin fractions (Fig 5B). RIOK3 knockdown had minimal effect on G-actin abundance. In contrast, siRIOK3 cells contained lower levels of F-actin in normoxia and even less in hypoxia, consistent with the reduced level of F-actin staining observed by confocal microscopy. Quantification of actin band density demonstrated a 45% reduction in the amount of F-actin in hypoxic siRIOK3 sample compared with hypoxic siCon cells (Fig 5C,  $P < 0.05$ ). The amount of TPM3 detected in F-actin fraction was similarly reduced with RIOK3 knockdown, supporting a role for RIOK3 in promoting the stability of TPM3-bound actin filaments.

### **RIOK3 expression is required for hypoxia-induced metastasis**

To investigate the role of RIOK3 in invasion and metastasis *in vivo* we utilised a zebrafish embryo model.<sup>31</sup> Following implantation into the perivitelline cavity of developing embryos, local and distal metastasis of MDA-MB-231 cells transfected with siRIOK3 was significantly reduced (arrowheads; Fig 6A). Quantification of disseminated cells and foci demonstrated a reduction from  $26 \pm 1.9/\text{embryo}$  for siCon cells to  $16 \pm 0.16/\text{embryo}$  for siRIOK3 cells (Fig 6B, mean  $\pm$  SD,  $n = 2$ ,  $P = 0.02$ ; t test).

The effect of RIOK3 on pulmonary metastasis was investigated following i.v. injection of MDA-MB-231 cells in SCID mice (Fig 6C). Normoxic shCon cells produced a metastatic burden of  $0.16 \pm 0.14\%$  human DNA (of total DNA) in the lungs at 9 weeks (mean  $\pm$  SEM,  $n = 7$ ). This was reduced in shRIOK3 cells to  $0.031 \pm 0.014\%$ . Exposure of cells to 24 h hypoxia *in vitro* prior to i.v. injection resulted in a significant increase of metastasis by 9-fold to  $1.5 \pm 0.42\%$  human DNA ( $P < 0.01$ ; one way ANOVA). This effect was suppressed in shRIOK3 cells to metastasis of  $0.17 \pm 0.018\%$  human DNA ( $P < 0.001$  vs. shCon hypoxia). These data suggest that the role of RIOK3 in cell invasion is also necessary for metastasis in animal models, particularly in the hypoxic induction of metastasis.

## Discussion

Metastasis is responsible for the majority of deaths due to breast cancer. The existence of intratumoural hypoxia is an important risk factor in the development of metastasis and, therefore, a better understanding of the molecular processes involved in hypoxia-driven metastasis is needed.

An extensive change in actin cytoskeletal organisation occurs when MDA-MB-231 cells are exposed to hypoxia. Despite this considerable remodelling, minimal overall difference in cell migration in 2D cell cultures is observed, with hypoxic cells migrating at similar velocity to normoxic cells, at least when exposed to 0.1% O<sub>2</sub>. In contrast, hypoxic MDA-MB-231 cells display a >5-fold enhanced ability to invade through 3D extracellular matrix, albeit at lower density than tumour tissue. This suggests that the altered hypoxic actin cytoskeleton is better optimised for invasive motility but provides little advantage in 2D movement. Actomyosin-dependent contraction is associated with stronger mechanical forces and is necessary for migration through 3D extracellular matrix, where forces generated at the rear of the cell squeeze the cell nucleus through the narrow gaps between connective tissue fibrils.<sup>32, 33</sup> In contrast, the protrusive forces generated at the leading edge of the cell by actin filament assembly and disassembly are sufficient for migration in 2D but do not provide sufficient mechanical force for invasion through 3D matrix. Our findings are consistent with a model whereby hypoxic modification of the actin cytoskeleton favours formation of longitudinal stress fibers and greater actomyosin contraction compared with a more dynamic and less contractile F-actin arrangement in normoxia.

It is recognised that myosin II is required for organisation of the actin cytoskeleton and establishment of cell polarisation. Myosin II is the dominant force generating motor in cells and promotes retraction of the cell rear during actin-based cell migration in most cell types.<sup>34</sup> MDA-MB-231 cells exclusively utilise a uropod containing F-actin/myosin-II at the rear of the cell to generate contractile forces necessary for invasion through 3D matrix.<sup>35</sup> We demonstrate that RIOK3 depletion causes MDA-MB-231 cells to become elongated because they fail to effectively protract their trailing edge (Fig 3D). This suggests that there is a lack of mechanical force generated at the rear of the cell and this defect results in an inability to invade through 3D matrix (Fig 3F). These observations implicate RIOK3 in maintenance of actomyosin contractility.

Depletion of RIOK3 resulted in changes in the organisation and abundance of F-actin (Fig 5). Tropomyosins are important regulators of actin fibers and can influence arrangement of stress fibers, lamellipodia and lamella and the rate of cell migration.<sup>12, 14</sup> We observed a reduction in the amount of TPM3 bound F-actin following RIOK3 depletion, particularly in hypoxic conditions. This change would be expected to reduce the stability of F-actin, as observed. RIOK3 was enriched in an area 2-4  $\mu\text{m}$  behind the leading edge of the migrating cell between the lamellopodium and lamella, located approximately 1-3  $\mu\text{m}$  and 4-11  $\mu\text{m}$  from the leading edge, respectively, in line with reported values.<sup>14</sup> High levels of the ARP2/3 complex are found in the lamellipodium where this complex promotes actin filament branching. ARP2 (ACTR2) was observed to co-immunoprecipitate with FLAG-RIOK3 suggesting that RIOK3 may function at the interface between the lamellipodium and

lamella to orchestrate specialisation of F-actin into a more linear TPM-bound lamellar conformation. Although this process is most clearly visualised at the leading edge of the cell these specialising effects on F-actin may also occur in other regions of the cell, contributing to the phenotype of defective protraction observed in cells with RIOK3 knockdown.

We demonstrated that RIOK3 knockdown reduced the level of pulmonary colonisation in an experimental model of pulmonary metastasis (Fig 6C). This assay only measures the late stages of metastasis i.e. extravasation and establishment of micrometastases and does not recapitulate all of the steps necessary for metastasis. Additional studies using orthotopic models are needed to better define the requirement of RIOK3 in the earlier steps of the metastatic cascade.

The development of HIF inhibitors is an on-going effort and may provide opportunities to reduce hypoxia-driven metastasis.<sup>36</sup> Given the modest and transient increase in RIOK3 protein expression during hypoxia, HIF inhibition is unlikely to significantly suppress RIOK3 expression. However, the re-localisation of RIOK3 that occurs in hypoxia suggests that it participates in the restructuring of the actin cytoskeleton that occurs during hypoxia, a process that is dependent on HIF1.<sup>37</sup> Our demonstration that RIOK3 is required for actin cytoskeletal organisation in both normoxia and hypoxia suggests that development of RIOK3 inhibitors to prevent cell invasion is a promising anti-invasion strategy. Further biochemical studies are needed to establish the kinase activity and substrates of RIOK3, and these efforts would aid in drug development projects.

## Materials and Methods

### Cell lines

MDA-MB-231 were obtained from ATCC (Lot: 5883183, cultures initiated 19/08/2010) and maintained in RPMI 1640 (Life Technologies, Paisley, UK) supplemented with 10% FBS (PAA Laboratories Ltd., Somerset, UK). HEK-293T cells were obtained from Open Biosystems (Lot: L0708; Thermo Scientific, Leicestershire, UK) and maintained in DMEM + 10% FBS. All studies were conducted using early passage cultures typically within 3 months of thawing from cell stocks confirmed mycoplasma negative.

### Hypoxic exposure

All hypoxic exposures were done at 0.1% O<sub>2</sub>/5% CO<sub>2</sub> in N<sub>2</sub> using an Invivo<sub>2</sub> 400 workstation (Ruskin Technology Ltd, Bridgend, UK).

### Real time-qPCR

RNA was extracted using TRI® reagent (Sigma-Aldrich) and converted to cDNA using a High Capacity cDNA Reverse Transcription Kit (Life Technologies). qPCR was carried out using SensiMix SYBR No-ROX One-Step Kit (BioLine, London, UK) using the following primers RIOK3 F AAGGAGTCTGTTGTCTTTCATGC, RIOK3 R CTTGATGGCACATTCTGTAGGT, HPRT1 F CCAGTCAACAGGGGACATAAA, HPRT1 R CACAATCAAGACATTCTTCCAGT.

## Western immunoblotting

Western immunoblotting was performed as reported.<sup>21</sup> Primary antibodies used were: RIOK3 (H00008780-M01, Abnova), HIF1 $\alpha$  (610959, BD Transduction Laboratories), HIF2 $\alpha$  (NB100-122; Novus), CA9 (clone M75, gift of J. Pastorek, Bratislava), TPM3 (ab113692, Abcam), TPM3 (HPA009066, Sigma-Aldrich), TMOD3 (HPA001849, Sigma-Aldrich) and Actin-HRP (A3854; Sigma-Aldrich). Band densitometry was performed using the Analyze Gels tool in ImageJ (<http://imagej.nih.gov/ij>, version 1.47q).

## RNAi

Cells were transfected with 20 nM siRNA targeting RIOK3 (SI02223396; siRIOK3) or AllStars Negative control (1027281; siCon) using HiPerFect reagent (Qiagen, Manchester, UK). Custom siRNA oligonucleotides containing 3 sequences targeting HIF-1 $\alpha$  (1 CAAGCAACTGTCATATATA, 2 TGCCACCACTGATGAATTA, 3 TGACTCAGCTATTCACCAA) or HIF-2 $\alpha$  (1 TAACGACCTGAAGATTGAA, 2 CAAGCCACTGAGCGCAAAT, 3 TGAATTCTACCATGCGCTA) were purchased from Eurogentec (Southampton, UK). pGIPZ plasmids targeting RIOK3 (Clone ID V2LHS\_16875; shRIOK3) or non-silencing control shRNAmir (RHS4743; shCon) were obtained from Thermo Scientific. Lentivirus packaging and titration was carried out as described.<sup>38</sup> Cells were transduced at MOI 1 and pools of transduced cells were selected with 1  $\mu$ g/mL puromycin (Life Technologies) 48 h post-transduction.

## Confocal microscopy

Cells grown on coverslips were rinsed in PBS, fixed in 4% (v/v) paraformaldehyde in PBS, permeabilised using 0.2% (v/v) Triton-X100 in PBS, blocked in 3% (w/v) BSA in PBS containing 0.1% Tween-20 (PBST) and incubated with primary antibody diluted in blocking buffer. Secondary detection utilised goat anti-mouse/rabbit IgG labelled with Alexa Fluor 488/594 (Life Technologies). F-actin was stained using 5  $\mu$ M TRITC-phalloidin (Sigma-Aldrich). DNA was stained using 1  $\mu$ M DAPI. Coverslips were mounted using ProLong<sup>®</sup> Gold antifade (Life Technologies). Confocal images were captured on a Zeiss 510 Inverted Confocal microscope using 63 $\times$  objective lens.

## *In vitro* 2D wound migration assay

MDA-MB-231 cells were seeded into Ibidi Culture-Inserts at 30,000 cells/well (Ibidi, Martinsried, Germany) and allowed to attach overnight. Inserts were removed and culture medium was aspirated and replaced. Images were captured at 3 marked sites/wound. Wound area (culture surface lacking cells) was measured using ImageJ. % wound remaining was calculated using the formula: wound at end h/wound at start $\times$ 100.

## Single cell migration in 2D

MDA-MB-231 were seeded in 24-well ImageLock Plates (Essen BioScience, Hertfordshire, UK). Cell migration was monitored on an Incucyte EX (Essen BioScience). Images in a series were opened in ImageJ, converted to stacks and then sorted on label. Cell movement was tracked manually using MTrackJ plugin.<sup>39</sup> Cells in clumps of >2 cells or those that

underwent cell division during assessment were excluded. >40 cells were analysed per sample.

### **Invasion assay**

100  $\mu$ L of 0.5 mg/mL Growth Factor Reduced Matrigel (BD Biosciences, Oxford, UK) was pipetted into 8  $\mu$ m pore size cell culture inserts (BD Bioscience) and allowed to set overnight.  $5 \times 10^4$  cells were seeded into the coated inserts in RPMI + 1% FBS and invasion was stimulated using RPMI + 10% FBS in the bottom chamber. At endpoint invaded cells were fixed with 4% formalin and stained with 0.5% crystal violet in H<sub>2</sub>O. Mean number of invaded cells/insert was assessed using 4 independent fields-of-view. % invasion was calculated using the formula: invaded cells/siCon normoxia invaded cells  $\times$  100.

### **FLAG immunoprecipitation**

Construction of the FLAG-RIOK3 expression construct is detailed in the supplementary methods. Immunoprecipitation was done using anti-FLAG® M2 magnetic beads (Sigma-Aldrich). Antigen and bound interacting species were eluted using either FLAG peptide or heating the beads to 70°C for 10 min in denaturing LDS buffer. Gels were stained using ProteoSilver™ Plus Silver Stain Kit (Sigma-Aldrich). Bands were excised from the gel, digested with trypsin and subjected to tandem mass spectrometry (LC-MS/MS) analysis as described previously.<sup>40</sup>

### **G-actin/F-actin fractionation assay**

Cellular G-actin/F-actin fractions were generated from samples containing  $1 \times 10^7$  cells using G-actin/F-actin In Vivo Assay Kit (Cytoskeleton Inc., Denver CO).

### **Zebrafish study**

Metastasis of MDA-MB-231 cells in the zebrafish embryo model was conducted as described.<sup>31</sup> Cells were transfected 24 hours prior to implantation into the perivitelline cavity.

### **Pulmonary metastasis assay**

6-8 week old female SCID (CB17/IcrHan®Hsd-Prkdc<sup>scid</sup> mice; Harlan, Bicester) were injected with  $2.5 \times 10^5$  cells (passed through a 40  $\mu$ m strainer) in 100  $\mu$ L RPMI into the tail vein. Cells in hypoxic groups were incubated for 24 h at 0.1% O<sub>2</sub> prior to harvest. At 9 weeks all mice were sacrificed and the lungs were frozen in liquid N<sub>2</sub>. All work was conducted in accordance with UK Home Office guidelines under project licence PPL30/2771.

### **Quantification of lung metastasis using qPCR**

Lung DNA was extracted using Gentra Puregene Tissue Kit (Qiagen). Standards of human and mouse DNA were generated from *in vitro* MDA-MB-231 cells and xenograft naïve mouse lung, respectively. Human specific or total (human + mouse) PTGER2 primer pairs were used to amplify 50 ng of lung DNA using syber green.<sup>41</sup> Samples containing 0.01, 0.1,

1, 10 or 100 ng human or mouse DNA were used to generate standard curves. Percent human DNA was calculated using the formula: human DNA/total DNA $\times$ 100.

### Statistical analysis

All statistical analyses were done using GraphPad Prism (v 6.0) by t test or one way ANOVA followed by Tukey's multiple comparisons test on independent experimental replicates, unless otherwise indicated (\* P < 0.05, \*\* P < 0.01, \*\*\* P < 0.001, \*\*\*\* P < 0.0001).

### Supplementary Material

Refer to Web version on PubMed Central for supplementary material.

### Acknowledgements

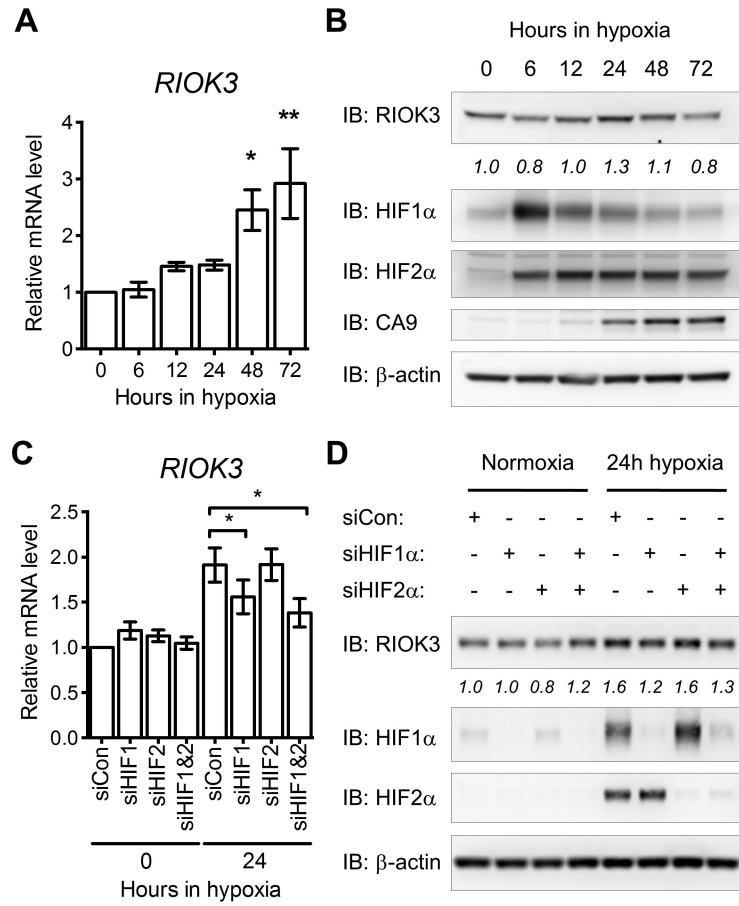
European Commission Metoxia Grant No. 222741 (D. Singleton, P. Rouhi, Y. Cao, A. Harris), Cancer Research UK (A. Harris, C. Zois, S. Haider, J. Li), Breast Cancer Research Foundation (A. Harris) and Oxford NIHR Biomedical Research Centre (B. Kessler). This study makes use of data generated by the Molecular Taxonomy of Breast Cancer International Consortium, which was funded by Cancer Research UK and the British Columbia Cancer Agency Branch.

### References

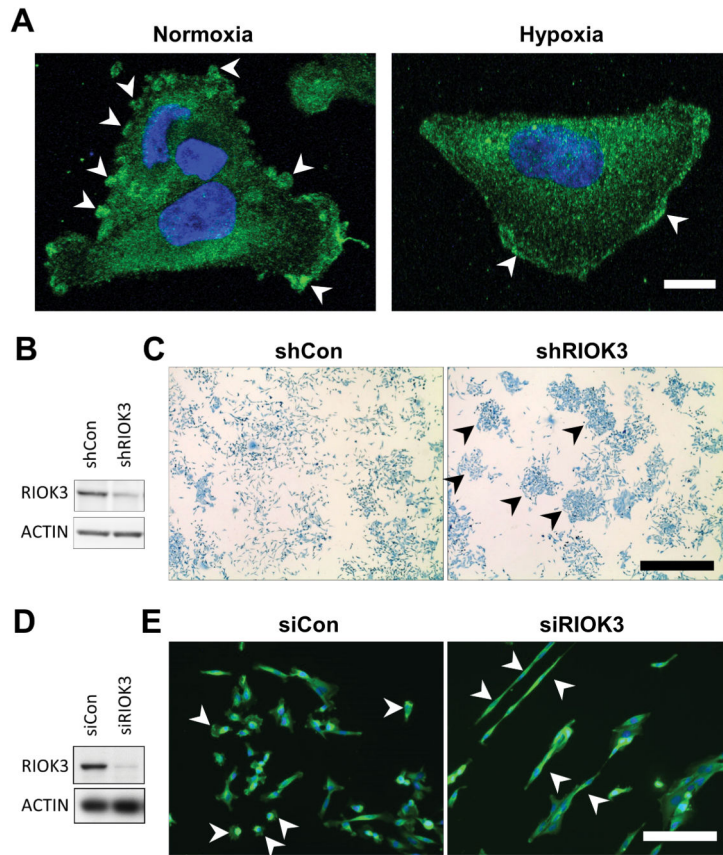
1. Elias AD. Triple-negative breast cancer: a short review. *Am J Clin Oncol*. 2010; 33:637–645. [PubMed: 20023571]
2. Vaupel P, Hockel M, Mayer A. Detection and characterization of tumor hypoxia using pO<sub>2</sub> histography. *Antioxid Redox Signal*. 2007; 9:1221–1235. [PubMed: 17536958]
3. Rundqvist H, Johnson RS. Hypoxia and metastasis in breast cancer. *Curr Top Microbiol Immunol*. 2010; 345:121–139. [PubMed: 20549469]
4. Dales JP, Garcia S, Meunier-Carpentier S, Andrac-Meyer L, Haddad O, Lavaut MN, et al. Overexpression of hypoxia-inducible factor HIF-1 $\alpha$  predicts early relapse in breast cancer: retrospective study in a series of 745 patients. *Int J Cancer*. 2005; 116:734–739. [PubMed: 15849727]
5. Yamamoto Y, Ibusuki M, Okumura Y, Kawasoe T, Kai K, Iyama K, et al. Hypoxia-inducible factor 1 $\alpha$  is closely linked to an aggressive phenotype in breast cancer. *Breast Cancer Res Treat*. 2008; 110:465–475. [PubMed: 17805961]
6. Erler JT, Bennewith KL, Nicolau M, Dornhofer N, Kong C, Le QT, et al. Lysyl oxidase is essential for hypoxia-induced metastasis. *Nature*. 2006; 440:1222–1226. [PubMed: 16642001]
7. Gilkes DM, Chaturvedi P, Bajpai S, Wong CC, Wei H, Pitcairn S, et al. Collagen prolyl hydroxylases are essential for breast cancer metastasis. *Cancer Res*. 2013; 73:3285–3296. [PubMed: 23539444]
8. Munoz-Najar UM, Neurath KM, Vumbaca F, Claffey KP. Hypoxia stimulates breast carcinoma cell invasion through MT1-MMP and MMP-2 activation. *Oncogene*. 2006; 25:2379–2392. [PubMed: 16369494]
9. Zhang H, Wong CC, Wei H, Gilkes DM, Korangath P, Chaturvedi P, et al. HIF-1-dependent expression of angiopoietin-like 4 and L1CAM mediates vascular metastasis of hypoxic breast cancer cells to the lungs. *Oncogene*. 2012; 31:1757–1770. [PubMed: 21860410]
10. Imai T, Horiuchi A, Wang C, Oka K, Ohira S, Nikaido T, et al. Hypoxia attenuates the expression of E-cadherin via up-regulation of SNAIL in ovarian carcinoma cells. *Am J Pathol*. 2003; 163:1437–1447. [PubMed: 14507651]
11. Pennacchietti S, Michieli P, Galluzzo M, Mazzone M, Giordano S, Comoglio PM. Hypoxia promotes invasive growth by transcriptional activation of the met protooncogene. *Cancer Cell*. 2003; 3:347–361. [PubMed: 12726861]

12. Ponti A, Machacek M, Gupton SL, Waterman-Storer CM, Danuser G. Two distinct actin networks drive the protrusion of migrating cells. *Science*. 2004; 305:1782–1786. [PubMed: 15375270]
13. Insall RH, Machesky LM. Actin dynamics at the leading edge: from simple machinery to complex networks. *Dev Cell*. 2009; 17:310–322. [PubMed: 19758556]
14. Gupton SL, Anderson KL, Kole TP, Fischer RS, Ponti A, Hitchcock-DeGregori SE, et al. Cell migration without a lamellipodium: translation of actin dynamics into cell movement mediated by tropomyosin. *J Cell Biol*. 2005; 168:619–631. [PubMed: 15716379]
15. Weber KL, Fischer RS, Fowler VM. Tmod3 regulates polarized epithelial cell morphology. *J Cell Sci*. 2007; 120:3625–3632. [PubMed: 17928307]
16. Tojkander S, Gateva G, Schevzov G, Hotulainen P, Naumanen P, Martin C, et al. A molecular pathway for myosin II recruitment to stress fibers. *Curr Biol*. 2011; 21:539–550. [PubMed: 21458264]
17. Baumas K, Soudet J, Caizergues-Ferrer M, Faublader M, Henry Y, Mouglin A. Human RioK3 is a novel component of cytoplasmic pre-40S pre-ribosomal particles. *RNA Biol*. 2012; 9:162–174. [PubMed: 22418843]
18. Widmann B, Wandrey F, Badertscher L, Wyler E, Pfannstiel J, Zemp I, et al. The kinase activity of human Rio1 is required for final steps of cytoplasmic maturation of 40S subunits. *Mol Biol Cell*. 2012; 23:22–35. [PubMed: 22072790]
19. Zemp I, Wild T, O'Donohue MF, Wandrey F, Widmann B, Gleizes PE, et al. Distinct cytoplasmic maturation steps of 40S ribosomal subunit precursors require hRio2. *J Cell Biol*. 2009; 185:1167–1180. [PubMed: 19564402]
20. Kimmelman AC, Hezel AF, Aguirre AJ, Zheng H, Paik JH, Ying H, et al. Genomic alterations link Rho family of GTPases to the highly invasive phenotype of pancreas cancer. *Proc Natl Acad Sci U S A*. 2008; 105:19372–19377. [PubMed: 19050074]
21. Rzymiski T, Milani M, Pike L, Buffa F, Mellor HR, Winchester L, et al. Regulation of autophagy by ATF4 in response to severe hypoxia. *Oncogene*. 2010; 29:4424–4435. [PubMed: 20514020]
22. Curtis C, Shah SP, Chin SF, Turashvili G, Rueda OM, Dunning MJ, et al. The genomic and transcriptomic architecture of 2,000 breast tumours reveals novel subgroups. *Nature*. 2012; 486:346–352. [PubMed: 22522925]
23. TCGA. Comprehensive molecular portraits of human breast tumours. *Nature*. 2012; 490:61–70. [PubMed: 23000897]
24. Buffa FM, Harris AL, West CM, Miller CJ. Large meta-analysis of multiple cancers reveals a common, compact and highly prognostic hypoxia metagene. *Br J Cancer*. 2010; 102:428–435. [PubMed: 20087356]
25. Carroll VA, Ashcroft M. Role of hypoxia-inducible factor (HIF)-1alpha versus HIF-2alpha in the regulation of HIF target genes in response to hypoxia, insulin-like growth factor-I, or loss of von Hippel-Lindau function: implications for targeting the HIF pathway. *Cancer Res*. 2006; 66:6264–6270. [PubMed: 16778202]
26. Hu CJ, Wang LY, Chodosh LA, Keith B, Simon MC. Differential roles of hypoxia-inducible factor 1alpha (HIF-1alpha) and HIF-2alpha in hypoxic gene regulation. *Mol Cell Biol*. 2003; 23:9361–9374. [PubMed: 14645546]
27. Raval RR, Lau KW, Tran MG, Sowter HM, Mandriota SJ, Li JL, et al. Contrasting properties of hypoxia-inducible factor 1 (HIF-1) and HIF-2 in von Hippel-Lindau-associated renal cell carcinoma. *Mol Cell Biol*. 2005; 25:5675–5686. [PubMed: 15964822]
28. Agus DB, Alexander JF, Arap W, Ashili S, Aslan JE, Austin RH, et al. A physical sciences network characterization of non-tumorigenic and metastatic cells. *Sci Rep*. 2013; 3:1449. [PubMed: 23618955]
29. LaRonde-LeBlanc N, Wlodawer A. A family portrait of the RIO kinases. *J Biol Chem*. 2005; 280:37297–37300. [PubMed: 16183636]
30. Koch A, Hauf S. Strategies for the identification of kinase substrates using analog-sensitive kinases. *Eur J Cell Biol*. 2010; 89:184–193. [PubMed: 20061049]
31. Rouhi P, Jensen LD, Cao Z, Hosaka K, Lanne T, Wahlberg E, et al. Hypoxia-induced metastasis model in embryonic zebrafish. *Nat Protoc*. 2010; 5:1911–1918. [PubMed: 21127485]

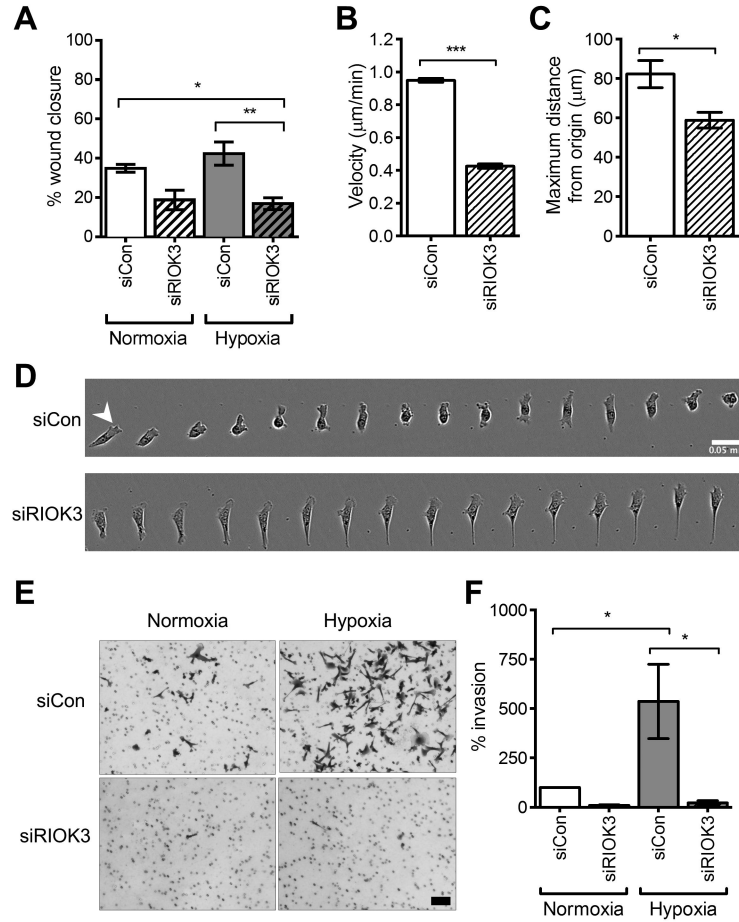
32. Lammermann T, Bader BL, Monkley SJ, Worbs T, Wedlich-Soldner R, Hirsch K, et al. Rapid leukocyte migration by integrin-independent flowing and squeezing. *Nature*. 2008; 453:51–55. [PubMed: 18451854]
33. Fournier MF, Sauser R, Ambrosi D, Meister JJ, Verkhovsky AB. Force transmission in migrating cells. *J Cell Biol*. 2010; 188:287–297. [PubMed: 20100912]
34. Cramer LP. Mechanism of cell rear retraction in migrating cells. *Curr Opin Cell Biol*. 2013; 25:591–599. [PubMed: 23764164]
35. Poincloux R, Collin O, Lizarraga F, Romao M, Debray M, Piel M, et al. Contractility of the cell rear drives invasion of breast tumor cells in 3D Matrigel. *Proc Natl Acad Sci U S A*. 2011; 108:1943–1948. [PubMed: 21245302]
36. Semenza GL. Hypoxia-inducible factors in physiology and medicine. *Cell*. 2012; 148:399–408. [PubMed: 22304911]
37. Weidemann A, Breyer J, Rehm M, Eckardt KU, Daniel C, Cicha I, et al. HIF-1 $\alpha$  activation results in actin cytoskeleton reorganization and modulation of Rac-1 signaling in endothelial cells. *Cell Commun Signal*. 2013; 11:80. [PubMed: 24144209]
38. Sims D, Mendes-Pereira AM, Frankum J, Burgess D, Cerone MA, Lombardelli C, et al. High-throughput RNA interference screening using pooled shRNA libraries and next generation sequencing. *Genome Biol*. 2011; 12:R104. [PubMed: 22018332]
39. Meijering E, Dzyubachyk O, Smal I. Methods for cell and particle tracking. *Methods Enzymol*. 2012; 504:183–200. [PubMed: 22264535]
40. Mackeen MM, Kramer HB, Chang KH, Coleman ML, Hopkinson RJ, Schofield CJ, et al. Small-molecule-based inhibition of histone demethylation in cells assessed by quantitative mass spectrometry. *J Proteome Res*. 2010; 9:4082–4092. [PubMed: 20583823]
41. Alcoser SY, Kimmel DJ, Borgel SD, Carter JP, Dougherty KM, Hollingshead MG. Real-time PCR-based assay to quantify the relative amount of human and mouse tissue present in tumor xenografts. *BMC Biotechnol*. 2011; 11:124. [PubMed: 22176647]



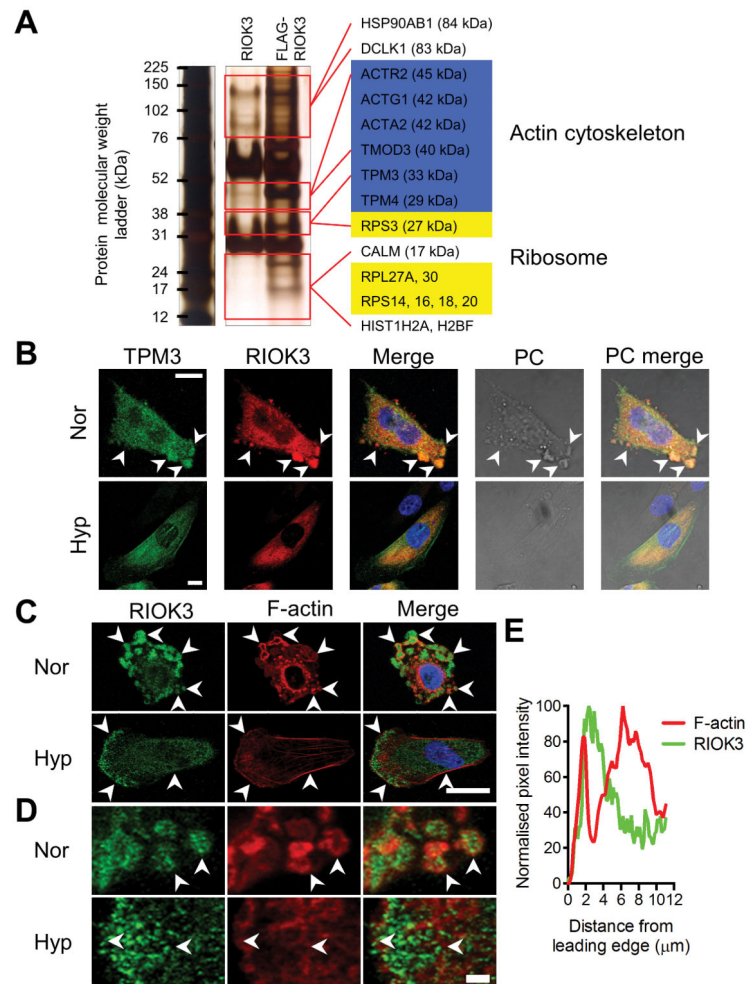
**Figure 1.** RIOK3 expression is increased in MDA-MB-231 cells during hypoxia in a HIF1α-dependent manner. (A) Expression of RIOK3 mRNA is increased in MDA-MB-231 cells during exposure to hypoxia (mean ± SEM, n = 3). (B) Expression of RIOK3 protein is transiently increased in MDA-MB-231 cells during exposure to hypoxia. Band density is indicated by italicised numbers below the immunoblot. HIF1α, HIF2α and CA9 immunoblots are presented as hypoxic controls. (C) The hypoxic up-regulation of RIOK3 mRNA in MDA-MB-231 cells is suppressed following transfection with siRNA targeting HIF1α or HIF1α and HIF2α (mean ± SEM, n = 4, repeated measures one-way ANOVA). (D) The hypoxic up-regulation of RIOK3 protein in MDA-MB-231 cells is suppressed following transfection with siRNA targeting HIF1α or HIF1α and HIF2α. Band density is indicated by italicised numbers below the immunoblot.



**Figure 2.** RIOK3 undergoes subcellular re-localisation in hypoxia and its depletion alters cell morphology. (A) Representative confocal images of migrating MDA-MB-231 cells in normoxia (Nor) or hypoxia (Hyp) stained for RIOK3. Scale bar = 10  $\mu$ m. (B) Immunoblot demonstrating RIOK3 expression in MDA-MB-231 cells transduced with shCon or shRIOK3 lentivirus. (C) shCon cells grow in a homogeneous, scattered pattern, whereas shRIOK3 cells form colonies after 1 week in culture (arrowheads). Scale bar = 1 mm. (D) Immunoblot demonstrating RIOK3 expression in MDA-MB-231 cells transfected with siCon or siRIOK3. (E) MDA-MB-231 cells immunofluorescently stained for RIOK3. Scale bar = 50  $\mu$ m.

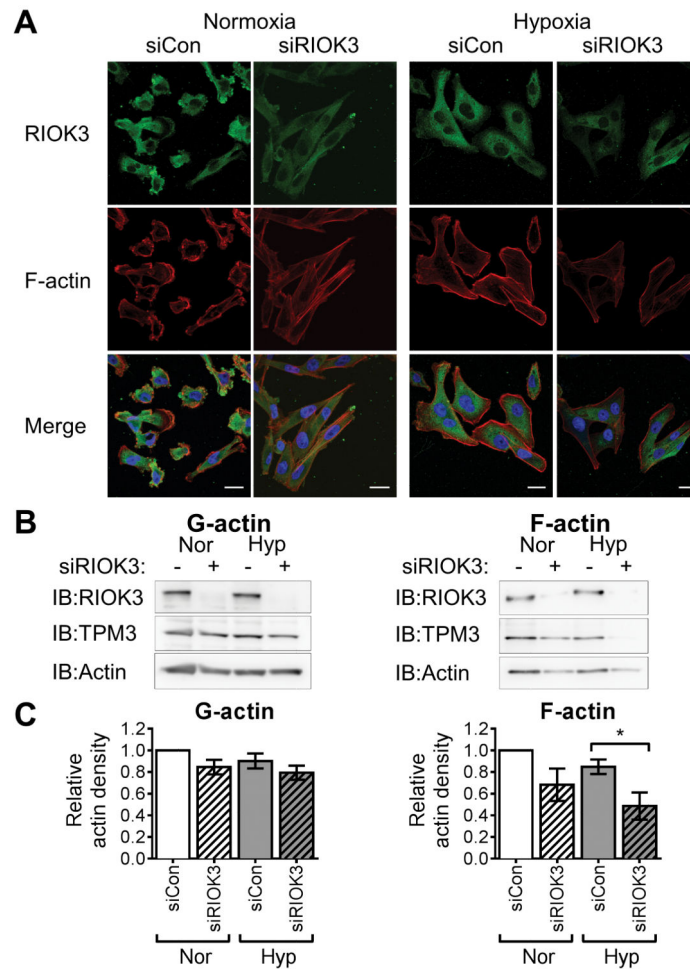


**Figure 3.** RIOK3 promotes 2D cell migration and 3D invasion in hypoxia. (A) Modified scratch wound assay shows the % wound area closed was decreased in normoxia and hypoxia following transfection of MDA-MB-231 cells with siRIOK3 (mean ± SEM, n = 4). (B-C) Analysis of single cell migration in 2D demonstrated cell velocity and maximum distance from origin were reduced in siRIOK3-transfected MDA-MB-231 cells (mean ± SEM, n = 3). (D) Timelapse image of migration of a single siCon or siRIOK3 transfected cell. Images were captured every 5 min over 75 min. Scale bar = 50 µm. (E) Representative 3D invasion assay micrographs. Scale bar = 0.2 mm (F) Cell invasion at 24 h is stimulated by hypoxia and this effect is suppressed in siRIOK3-transfected cells. Columns represent invaded cells as a % of siCon normoxia (mean ± SEM, n = 3).



**Figure 4.**

RIOK3 associates with TPM3 and actin in cells. (A) Silver-stained PAGE gel of anti-FLAG immunoprecipitates from MDA-MB-231 cells expressing either RIOK3 or FLAG-RIOK3. Species detected by tandem mass spectrometry only in the FLAG-RIOK3 sample are indicated on the right of the gel by gene symbol. (B) Confocal images of MDA-MB-231 cells in normoxia (Nor) and hypoxia (Hyp) demonstrate colocalisation of RIOK3 and TPM3. Scale bar = 10  $\mu\text{m}$ . Phase contrast (PC) images show changes in cellular appearance. (C) Confocal images of MDA-MB-231 cells demonstrate that RIOK3 associates with actin. In normoxia RIOK3 aggregates are often surrounded by F-actin (arrowheads). In hypoxia RIOK3 aggregates disperse and F-actin organisation changes to form stress fibers and a dense F-actin network adjacent to the leading edge (arrowheads). Scale bar = 20  $\mu\text{m}$ . (D) Magnified images of regions in C. Scale bar = 2  $\mu\text{m}$ . (E) Pixel density of F-actin and RIOK3 stain at the leading edge of the hypoxic cell (from D). F-actin is observed immediately adjacent to the cell edge, followed by an intense band of RIOK3 stain and then a wider band of F-actin.

**Figure 5.**

RIOK3 promotes F-actin stability in cells. (A) Confocal microscopy images of MDA-MB-231 cells transfected with siRIOK3 demonstrate reduced F-actin stain and altered organisation in both normoxia and hypoxia. All images were captured using the same exposure settings to enable comparison. Scale bar = 20  $\mu$ m. (B) Levels of G- and F-actin in MDA-MB-231 cells following RIOK3 knockdown. The amount of F-actin was reduced in siRIOK3-transfected cells in both normoxia and hypoxia. The levels of TPM3 in the F-actin fraction were also reduced in siRIOK3-transfected cells, particularly in hypoxic conditions. (C) Relative actin band density for G- and F-actin fractions (mean  $\pm$  SEM, n = 3).

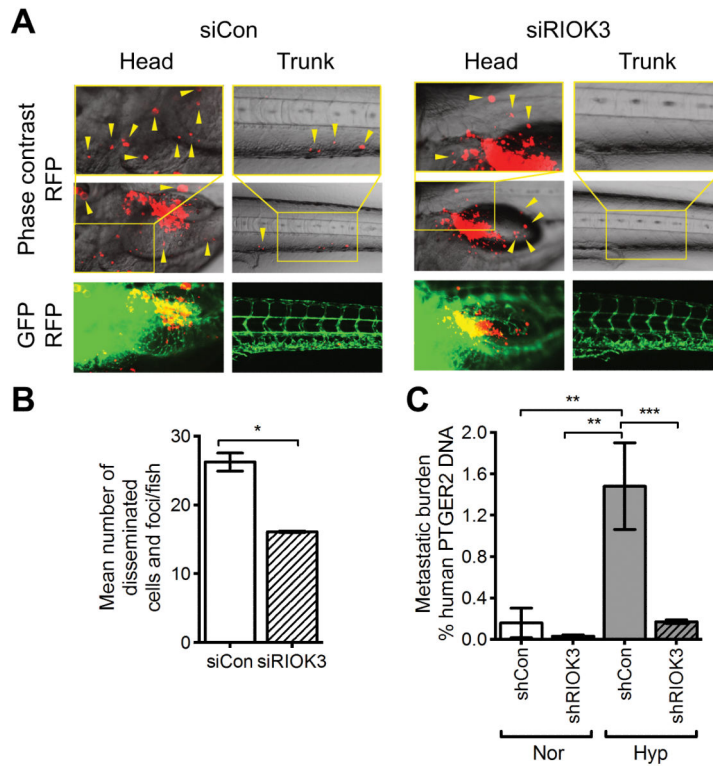


**Figure 6.** RIOK3 expression is required for metastasis in zebrafish and mouse models. (A) Dissemination and metastasis of MDA-MB-231 cells in zebrafish embryos. Cells were implanted into 48 h post-fertilization zebrafish embryos and then detected at day 4 post-injection. Arrowheads indicate disseminated tumour cells and foci. (B) Mean number of disseminated cells/foci was quantified in >20 embryos (n = 2; mean ± SD). (C) Metastatic burden in lungs following i.v. injection of MDA-MB-231 cells with or without 24 h prior hypoxic exposure (n = 7 mice/group; mean ± SEM).